

Instantaneous Failure, Repair and Mobility Rates for Markov Reliability Systems: A Wind-Farm application

Guglielmo D'Amico, Filippo Petroni*

Dipartimento di Economia, Università 'G. d'Annunzio' Chieti-Pescara, viale Pindaro 42, Pescara, 65127, Italy

ARTICLE INFO

Keywords:
Markov processes
Reliability
mobility measures

ABSTRACT

The Rate of Occurrence of Failures (ROCOF) is a widely utilized indicator for assessing a system's performance over time, yet it does not fully disclose the instantaneous behavior of a system. This paper introduces new measures to complement the ROCOF, providing a more comprehensive understanding of system reliability, particularly for Markov systems. We define the Rate of Occurrence of Repairs (ROCOR), which quantifies the system's instantaneous tendency to transition from failure to working states, and the Rate of Inoccurrence (ROI), which measures the propensity to remain within the current subset of states (either working or failure) without transitioning out. Explicit expressions for the computation of these rates are derived for Markov systems. Furthermore, a Total Mobility Rate (TMR) is proposed, integrating these individual rates to capture the overall dynamism of the system. The utility of these new indicators is demonstrated through a significant real-world application to wind farm management. The results from the wind farm study show that ROCOR, ROI, and TMR, when used in conjunction with ROCOF, reveal nuanced operational dynamics and reliability characteristics that are not discernible from static measures like Weibull parameters or ROCOF alone. These indicators can distinguish between sites with similar long-term wind profiles by identifying different "reliability logics," such as persistence-driven versus transition-driven behaviors. This enriched, time-dependent perspective provides valuable information for maintenance scheduling, operational strategies, and risk assessment, ultimately enhancing the ability to manage complex systems effectively.

1. Introduction

The body of literature on reliability theory and its applications is extensive and continues to grow, driven by ongoing efforts to more accurately characterize system behavior and enhance usability, safety, and overall performance e.g., Blichke and Murthy (2011); Barbu and Limnios (2009).

Reliability is a probabilistic concept related to the random evolution of a system. Therefore, in all reliability investigations, it is necessary to start with a description of the system's behaviour according to a stochastic model (see, e.g. Ushakov (2012)). Many alternatives are possible, but a predominant role is played by multistate models. This class of mathematical models assumes that the system's functioning can be described by a set of states, and transitions are possible among some of them. The probability of the occurrence of transitions is modeled according to different types of stochastic processes, such as Markov and semi-Markov ones; see, e.g., Koutras (1996); Limnios and Oprisan (2001). The semi-Markov case is of particular relevance, both theoretically and practically. Indeed, contrary to the Markov case, where the sojourn time in a state is restricted to being geometrically or exponentially distributed, these processes have sojourn times in states that can be of arbitrary type.

Even when a simple model is considered, that is, a few states and a simple dynamic evolution between them, understanding the system requires the adoption of different indicators that highlight specific aspects of interest. The reliability function is one of the most important indicators and has been extensively studied. It expresses the probability of not experiencing any failure in a given period of time. This notion was generalized considering the interval measures introduced by Csenki (1994, 1995) for continuous-time processes; its discrete counterpart was studied in Georgiadis and Limnios (2014, 2016). In Barbu, D'Amico, and Gkelsinis (2021); D'Amico and Gkelsinis (2024) a

The Authors acknowledge financial support from the European Union - NextGenerationEU program, Missione 4 Componente 1, CUP D53D23006470006, MUR PRIN 2022 n. 2022ETEHRM "Stochastic models and techniques for the management of wind farms and power systems" by the Italian Ministero dell'Università e della Ricerca.

*Corresponding author

✉ g.damico@unich.it (G. D'Amico); filippo.petroni@unich.it (F. Petroni)
ORCID(s):

further generalization in this line of research was given with the notion of sequential interval reliability, which expresses the probability that the system works in a sequence of nonoverlapping time intervals.

Other metrics, such as availability and maintainability functions, are commonly computed for Markov systems (see, e.g. Platis, Limnios, and Le Du (1998)) and semi-Markov ones (see, e.g. Limnios (1997)) with generalizations to duration-dependent measures (D'Amico, Janssen, and Manca (2010); D'Amico, Manca, Petroni, and Selvamuthu (2021)).

Previous concepts and results found generalizations for systems with a continuous state space allowing for both discrete and continuous stochastic performance degradations; see, e.g., Yang and Xue (1996); D'Amico (2011); Limnios (2012).

The measures discussed above quantify the system evolution over a given period of time. Nevertheless, in addition to these measures, it is very frequent to compute failure rates, as they express the instantaneous propensity to experience a failure given that the system has already survived to the current time. Among the instantaneous measures, the ROCOF has attracted the interest of many researchers. The ROCOF is defined as the time derivative of the expected number of failures. Confining our attention to the ROCOF of multi-state systems, it is worth mentioning two research articles by Yeh Lam (Yeh (1995); Yang and Xue (1996)) where the author derives a formula for the ROCOF of a continuous-time Markov chain of higher dimension after having introduced additional variables. These results have been extended to the semi-Markov setting by Ouhbi and Limnios (2002) and a new indicator, named n -ROCOF (rate of occurrence of failure of order n) was proposed and studied by D'Amico (2015) for continuous-time Markov chains and by D'Amico and Petroni (2023) for semi-Markov processes. More information on this research stream can be found in D'Amico and Gismondi (2024) where a review of the ROCOF of multi-state systems with application has been proposed.

The ROCOF is a very informative measure, but it is not able to completely disclose the instantaneous behavior of a system. For this reason, we introduce two auxiliary measures that share ideas similar to those of the ROCOF but focus on different events. First, we introduce the rate of occurrence of repairs (ROCOR). This measure represents the instantaneous tendency of the system to experience a repair, that is, a transition from the subset of failure states to the one of working states. Hence, the ROCOR provides valuable information on the capacity of the system to recover its good working conditions. We show that there may be systems that share a similar shape of the ROCOF function but differ from each other when the ROCOR is computed. Second, we define another measure, which we call the rate of inoccurrence (ROI). It gives information on the instantaneous propensity of the system to not experience failures or repairs. The relationship between these three rates is identified. Although in this work we do not attempt to quantify resilience in the cumulative sense of Bruneau, Chang, Eguchi, Lee, O'Rourke, Reinhorn, Shinozuka, Tierney, Wallace, and Von Winterfeldt (2003) and Sharma, Tabandeh, and Gardoni (2018), the mobility rates introduced here constitute the instantaneous components of any such resilience calculation, providing a real-time view of the system's tendency to fail, recover, or persist.

Third, by summing the three previously defined reliability indices, we introduce a new metric called the Total Mobility Rate. This index reflects the system's overall tendency to transition between states, regardless of how the state space is partitioned into working and fault states. As such, the total mobility rate can also be applied to other domains where such a clear-cut distinction between states does not exist, extending its usefulness beyond traditional reliability analysis.

Finally, we describe the results of a real application in the wind energy domain, where the proposed indicators are computed for 18 wind farms located in diverse climatic regions across the globe. Using hourly MERRA-2 wind speed data, we estimate the generator matrix and compute the Rate of Occurrence of Failures (ROCOF), Rate of Occurrence of Repairs (ROCOR), Rate of Inoccurrence (ROI), and Total Mobility Rate (TMR). The results reveal significant differences among sites, even when Weibull parameters are similar, highlighting distinct reliability profiles: persistence-driven systems with low TMR and highly dynamic sites characterized by frequent state transitions. This analysis provides new insights for operational strategies and reliability classification of wind power systems.

The paper proceeds as follows. Section 2 describes the basic reliability problem related to Markov processes and presents the three rate functions and their evaluation formulas. Section 3 provides a detailed analysis of an application to. In Section 4, we review the content of the paper and provide general conclusions.

2. Markov processes and Reliability analysis

Markov processes are frequently used in the modeling of a system and, consequently, in its reliability analysis; see Billinton and Bollinger (1968); Banjevic and Jardine (2006); Csenki (2007).

In this section, we briefly introduce their main characteristics related to the reliability problem. Detailed information can be found in specific textbooks on stochastic processes; see, e.g., Brémaud (1999).

Consider a continuous-time Markov process $\{X(t), t \in \mathbb{R}_+\}$ with a finite state space $E = \{1, 2, \dots, s\}$. The probabilistic evolution of the system is given by a set of transition probability functions defined $\forall i, j \in E$ as

$$P_{i,j}(t) = \mathbb{P}[X(t) = j | X(0) = i], \quad (1)$$

with $P_{i,i}(0) = 1$ and $P_{i,j}(0) = 0$.

In the time-homogeneous framework, these transition probability functions are invariant with respect to time translations; hence $\forall s$, it results that

$$\mathbb{P}[X(t+s) = j | X(s) = i] = \mathbb{P}[X(t) = j | X(0) = i] = P_{i,j}(t).$$

The dynamic of the process is fully described by a vector of initial probabilities

$$\alpha_i := \mathbb{P}[X(0) = i], \quad i \in E, \quad \sum_{j \in E} \alpha_j = 1,$$

and a generator matrix $\mathbf{Q} = (q_{i,j})_{i,j \in E}$ such that $q_{i,j} \geq 0, \forall i \neq j$ and $q_{i,i} = -\sum_{j \neq i} q_{i,j}$. The elements of the generator have a probabilistic interpretation in terms of transition rates

$$q_{i,j} = \lim_{t \rightarrow 0} \frac{P_{i,j}(t)}{t}, \quad i \neq j, \quad q_{i,i} = \lim_{t \rightarrow 0} \frac{P_{i,i}(t) - 1}{t}.$$

Let $\mathbf{P}(t) = (P_{i,j}(t))$ be the matrix of the transition probability functions. Matrix $\mathbf{P}(t)$ satisfy two systems of differential equations, which, written in matrix form, are

$$\dot{\mathbf{P}}(t) = \mathbf{P}(t) * \mathbf{Q} \quad \text{and} \quad \dot{\mathbf{P}}(t) = \mathbf{Q} * \mathbf{P}(t).$$

They are called forward and backward Kolmogorov equations, respectively. It is well known that

$$e^{t\mathbf{Q}} := \sum_{k=0}^{\infty} \frac{\mathbf{Q}^k t^k}{k!}$$

is the unique solution to both Kolmogorov equations. Thus,

$$P_{i,j}(t) = \left(e^{t\mathbf{Q}} \right)_{i,j}.$$

Now, the unconditional probability of finding the process at time t in any state j can be easily computed:

$$p_j(t) := \mathbb{P}[X(t) = j] = \sum_{i \in E} \alpha_i P_{i,j}(t). \quad (2)$$

Transition probability functions are used to measure the performance of the system, as the different reliability indicators depend on the probabilistic behavior of the system. To do this, usually the state space E is partitioned into two disjoint non-empty subsets W and F . The former denotes the set of working states in which the system is operational at different levels; the latter collects all states, denoting a failure of different sizes. Without loss of generality, let us assume that the first m of s states work and the remaining ones are fault states, i.e.

$$W = \{1, 2, \dots, m\}, \quad \text{and} \quad F = \{m+1, m+2, \dots, s\}.$$

Among the main performability measures, we can mention the availability and reliability functions. The following formulas provide the definitions of these indicators and their computational formulas. More details can be found in Sadek and Limnios (2005) including their non-parametric estimation problem.

Consider the following block representation of the generator matrix and of the initial probability vector:

$$\mathbf{Q} = \begin{pmatrix} \mathbf{Q}_{WW} & \mathbf{Q}_{WF} \\ \mathbf{Q}_{FW} & \mathbf{Q}_{FF} \end{pmatrix} \quad \alpha = [\alpha_W, \alpha_F],$$

where \mathbf{Q}_{WW} denotes the block of the generator matrix that contains only the transition rates between couples of working states; a similar interpretation can be given for the other blocks. Furthermore, we denote by $\mathbf{1}_{s,m}$ the s -dimensional column vector whose m first elements are equal to one and the remaining $s - m$ are null.

The availability function can be defined and evaluated according to the following equation:

$$A(t) := \mathbb{P}[X(t) \in W] = \boldsymbol{\alpha} * (e^{t\mathbf{Q}}) * \mathbf{1}_{s,m}. \quad (3)$$

Equation (3) expresses the probability of finding the system working at time t .

The reliability function can be defined and evaluated according to the following equation:

$$R(t) := \mathbb{P}[X(u) \in W, \forall s \in [0, t]] = \boldsymbol{\alpha}_W * (e^{t\mathbf{Q}_{WW}}) * \mathbf{1}_{m,m}. \quad (4)$$

Equation (4) expresses the probability of finding the system working at any time u between zero and t .

2.1. ROCOF and related measures

The rate of occurrence of failure (ROCOF) is one of the most commonly utilized indicators available for assessing a system's performance over time. The ROCOF is the time derivative of the expected number of failures up to time t . To formalise this concept, we introduce the process $N_f(t)$ that denotes the number of system failures until time t .

Definition 1. *The ROCOF at time t for a Markov process, denoted by $rof(t)$, is defined by*

$$rof(t) := \lim_{\Delta t \rightarrow 0} \frac{\mathbb{E}[N_f(t + \Delta t) - N_f(t)]}{\Delta t}. \quad (5)$$

The ROCOF has been computed for a Markov process system for the first time in Ding-hua (1985) and successively analyzed for denumerable Markov processes in Yeh (1997). The following result shows how to compute the ROCOF.

Theorem 2 (Ding-hua (1985)). *The ROCOF function of a Markov process of generator matrix \mathbf{Q} and vector of initial probabilities $\boldsymbol{\alpha}$ is given by*

$$rof(t) = \sum_{i \in E} \sum_{w \in W} \sum_{f \in F} \alpha_i (e^{t\mathbf{Q}})_{i,w} \cdot q_{w,f}. \quad (6)$$

This indicator offers an understanding of the frequency of failure occurrences. Increasing values of it are evidence of a system that is going to deteriorate, while decreasing values show improvement in the system's performance.

Based on the same intuition that generates the ROCOF and its analysis, it is possible to advance a symmetric indicator focussing on repair events rather than failures. To this end, let us introduce the counting process $N_r(t)$, which denotes the number of repairs by time t .

Definition 3. *The rate of occurrence of repair (ROCOR) at time t for a Markov process, denoted by $ror(t)$, is defined by*

$$ror(t) := \lim_{\Delta t \rightarrow 0} \frac{\mathbb{E}[N_r(t + \Delta t) - N_r(t)]}{\Delta t}. \quad (7)$$

The ROCOR can be computed for a Markov process using symmetric arguments such as those advanced in Ding-hua (1985) and Yeh (1997). It is sufficient to exchange the set of working states with that of failure states. For this reason, we directly show the next results without giving a proof, which is elementary.

Theorem 4. *The ROCOR function of a Markov process of generator matrix \mathbf{Q} and vector of initial probabilities $\boldsymbol{\alpha}$ is given by*

$$ror(t) = \sum_{i \in E} \sum_{f \in F} \sum_{w \in W} \alpha_i (e^{t\mathbf{Q}})_{i,f} \cdot q_{f,w}. \quad (8)$$

This indicator offers an understanding of the frequency of repair occurrences. Increasing values of it are evidence of a system that is going to be repaired frequently, while decreasing values show that it is becoming more difficult for the system to be repaired.

The complete description of the system behavior needs an auxiliary process that complements the information provided by the ROCOF and the ROCOR indicators. This process should be able to measure the tendency of the system to not experience any failure or repair, that is, the tendency to not exit from the subset to which it currently belongs. To this end, we introduce a third process $N_i(t)$ that counts the number of transitions within the same subsets of states, that is, from every state of $w \in W$ to any different state $w_1 \in W$ and from every state of $f \in F$ to any different state $f_1 \in F$. Clearly, the following relationship holds:

$$N(t) = N_f(t) + N_r(t) + N_i(t).$$

Definition 5. The rate of inoccurrence (ROI) at time t for a Markov process, denoted by $roi(t)$, is defined by

$$roi(t) := \lim_{\Delta t \rightarrow 0} \frac{\mathbb{E}[N_i(t + \Delta t) - N_i(t)]}{\Delta t}. \quad (9)$$

Theorem 6. The ROI function of a Markov process of generator matrix \mathbf{Q} and vector of initial probabilities $\boldsymbol{\alpha}$ is given by

$$roi(t) = \sum_{i \in E} \left(\sum_{w \in W} \sum_{W \ni w_1 \neq w} \alpha_i(e^{\mathbf{Q}t})_{i,w} \cdot q_{w,w_1} + \sum_{f \in F} \sum_{F \ni f_1 \neq f} \alpha_i(e^{\mathbf{Q}t})_{i,f} \cdot q_{f,f_1} \right). \quad (10)$$

PROOF. The proof is composed of three main parts. First, we are going to prove that

$$roi(t) := \lim_{\Delta t \rightarrow 0} \frac{\mathbb{E}[N_i(t + \Delta t) - N_i(t)]}{\Delta t} = \lim_{\Delta t \rightarrow 0} \frac{\mathbb{P}[dN_i(t) = 1]}{\Delta t}, \quad (11)$$

where $dN_i(t) := N_i(t + \Delta t) - N_i(t)$.

Clearly,

$$\begin{aligned} \mathbb{E}[N_i(t + \Delta t) - N_i(t)] &= \sum_{k \geq 1} k \mathbb{P}[N_i(t + \Delta t) - N_i(t) = k] \\ &= \mathbb{P}[dN_i(t) = 1] + \sum_{k \geq 2} k \mathbb{P}[dN_i(t) = k]. \end{aligned}$$

Set $q = \max_{i \in E} \sum_{j \neq i} q_{i,j}$ and observe that

$$\mathbb{P}[dN_i(t) = k] \leq \mathbb{P}[dN(t) \geq k] \leq (q \cdot \Delta t)^k,$$

where the last inequality follows from Lemma 1 in Yeh (1997). Thus, we have

$$\begin{aligned} \mathbb{P}[dN_i(t) = 1] &\leq \mathbb{E}[N_i(t + \Delta t) - N_i(t)] \leq \mathbb{P}[dN_i(t) = 1] + \sum_{k \geq 2} k \mathbb{P}[dN(t) = k] \\ &\leq \mathbb{P}[dN_i(t) = 1] + \sum_{k \geq 2} k(q \cdot \Delta t)^k = \mathbb{P}[dN_i(t) = 1] + o(\Delta t). \end{aligned}$$

It follows

$$\lim_{\Delta t \rightarrow 0} \frac{\mathbb{P}[dN_i(t) = 1]}{\Delta t} \leq \lim_{\Delta t \rightarrow 0} \frac{\mathbb{E}[N_i(t + \Delta t) - N_i(t)]}{\Delta t} \leq \lim_{\Delta t \rightarrow 0} \frac{\mathbb{P}[dN_i(t) = 1]}{\Delta t} + \lim_{\Delta t \rightarrow 0} \frac{o(\Delta t)}{\Delta t}, \quad (12)$$

from which equation (11) follows.

As a second step, we provide a representation of $\lim_{\Delta t \rightarrow 0} \frac{\mathbb{P}[dN_i(t)=1]}{\Delta t}$ that can be efficiently computed.

Consider

$$\mathbb{P}[dN_f(t) = 0, dN_r(t) = 0]$$

$$= \mathbb{P}[dN_f(t) = 0, dN_r(t) = 0, T_{N(t)+1} - t > \Delta t] + \mathbb{P}[dN_f(t) = 0, dN_r(t) = 0, T_{N(t)+1} - t \leq \Delta t].$$

We notice that

$$\mathbb{P}[dN_f(t) = 0, dN_r(t) = 0, T_{N(t)+1} - t > \Delta t] = \mathbb{P}[T_{N(t)+1} - t > \Delta t],$$

and

$$\mathbb{P}[dN_f(t) = 0, dN_r(t) = 0, T_{N(t)+1} - t \leq \Delta t] = \mathbb{P}[dN_i(t) \geq 1].$$

Next, we observe that

$$\mathbb{P}[dN_i(t) \geq 1] = \mathbb{P}[dN_i(t) = 1] + \mathbb{P}[dN_i(t) \geq 2] \leq \mathbb{P}[dN_i(t) = 1] + (q \cdot \Delta t)^2.$$

Then, divide by Δt , let $\Delta t \rightarrow 0$, and observe that $\lim_{\Delta t \rightarrow 0} \frac{(q \cdot \Delta t)^2}{\Delta t} = 0$. Hence, we have

$$\begin{aligned} \lim_{\Delta t \rightarrow 0} \frac{1}{\Delta t} \mathbb{P}[dN_f(t) = 0, dN_r(t) = 0] \\ = \lim_{\Delta t \rightarrow 0} \frac{1}{\Delta t} \mathbb{P}[T_{N(t)+1} - t > \Delta t] + \lim_{\Delta t \rightarrow 0} \frac{1}{\Delta t} \mathbb{P}[dN_i(t) = 1]. \end{aligned}$$

We can also write the previous relationship as

$$\lim_{\Delta t \rightarrow 0} \frac{1}{\Delta t} \mathbb{P}[dN_i(t) = 1] = \lim_{\Delta t \rightarrow 0} \frac{1}{\Delta t} \left(\mathbb{P}[dN_f(t) = 0, dN_r(t) = 0] - \mathbb{P}[T_{N(t)+1} - t > \Delta t] \right). \quad (13)$$

To complete the proof, we must evaluate the probability on the right-hand side of equation (13). Owing to the Markovian property, $X(t)$ we have

$$\begin{aligned} \mathbb{P}[T_{N(t)+1} - t > \Delta t] &= \sum_{i \in E} \sum_{j \in E} \mathbb{P}[X(t) = j, T_{N(t)+1} - t > \Delta t | X(0) = i] \cdot \mathbb{P}[X(0) = i] \\ &= \sum_{i \in E} \sum_{j \in E} \alpha_i \cdot \mathbb{P}[T_{N(t)+1} - t > \Delta t | X(t) = j] \cdot \mathbb{P}[X(t) = j | X(0) = i] \\ &= \sum_{i \in E} \sum_{j \in E} \alpha_i \cdot \left(e^{t\mathbf{Q}} \right)_{i,j} \cdot e^{-q_j \Delta t}. \end{aligned}$$

Observe that as $\Delta t \rightarrow 0$ the use of the first-order Taylor expansion gives $e^{-q_j \Delta t} = 1 - q_j \Delta t + o(\Delta t)$, thus the former equation becomes equal to

$$\begin{aligned} &= \sum_{i \in E} \sum_{j \in E} \alpha_i \cdot \left(e^{t\mathbf{Q}} \right)_{i,j} \cdot [1 - q_j \Delta t + o(\Delta t)] \\ &= \sum_{i \in E} \sum_{j \in E} \alpha_i \cdot \left(e^{t\mathbf{Q}} \right)_{i,j} - \sum_{i \in E} \sum_{j \in E} \alpha_i \cdot \left(e^{t\mathbf{Q}} \right)_{i,j} \cdot q_j \Delta t + o(\Delta t) \\ &= 1 - \sum_{i \in E} \sum_{j \in E} \alpha_i \cdot \left(e^{t\mathbf{Q}} \right)_{i,j} \cdot q_j \Delta t + o(\Delta t). \end{aligned} \quad (14)$$

Next consider the probability

$$\begin{aligned} &\mathbb{P}[dN_f(t) = 0, dN_r(t) = 0] \\ &= \sum_{w \in W} \mathbb{P}[dN_f(t) = 0, dN_r(t) = 0 | X(t) = w] \cdot \mathbb{P}[X(t) = w] \\ &+ \sum_{f \in F} \mathbb{P}[dN_f(t) = 0, dN_r(t) = 0 | X(t) = f] \cdot \mathbb{P}[X(t) = f]. \end{aligned} \quad (15)$$

Now observe that using equation (13) we have that

$$\mathbb{P}[dN_f(t) = 0, dN_r(t) = 0 | X(t) = w]$$

$$\begin{aligned}
 &= \mathbb{P}[dN(t) = 0 | X(t) = w] + \mathbb{P}[dN_i(t) \geq 1 | X(t) = w] \\
 &= \mathbb{P}[T_{N(t)+1} - t > \Delta t | X(t) = w] + \mathbb{P}[dN_i(t) = 1 | X(t) = w] + o(\Delta t) \\
 &= 1 - q_w \Delta t + \sum_{W \ni w_1 \neq w} q_{w,w_1} \Delta t + o(\Delta t).
 \end{aligned} \tag{16}$$

Similarly,

$$\mathbb{P}[dN_f(t) = 0, dN_r(t) = 0 | X(t) = f] = 1 - q_f \Delta t + \sum_{F \ni f_1 \neq f} q_{f,f_1} \Delta t + o(\Delta t). \tag{17}$$

Substituting (16) and (17) into equation (15), we get

$$\begin{aligned}
 &\mathbb{P}[dN_f(t) = 0, dN_r(t) = 0] \\
 &= \sum_{w \in W} [1 - q_w \Delta t + \sum_{W \ni w_1 \neq w} q_{w,w_1} \Delta t + o(\Delta t)] \cdot p_w(t) \\
 &+ \sum_{f \in F} [1 - q_f \Delta t + \sum_{F \ni f_1 \neq f} q_{f,f_1} \Delta t + o(\Delta t)] \cdot p_f(t).
 \end{aligned} \tag{18}$$

Finally, by replacing (14) and (18) into equation (13), we can write the $\text{roi}(t)$ function as follows:

$$\begin{aligned}
 \text{roi}(t) &= \lim_{\Delta t \rightarrow 0} \frac{1}{\Delta t} \left\{ \sum_{w \in W} [1 - q_w \Delta t + \sum_{W \ni w_1 \neq w} q_{w,w_1} \Delta t + o(\Delta t)] \cdot p_w(t) \right. \\
 &+ \sum_{f \in F} [1 - q_f \Delta t + \sum_{F \ni f_1 \neq f} q_{f,f_1} \Delta t + o(\Delta t)] \cdot p_f(t) \\
 &\left. - 1 + \sum_{i \in E} \sum_{j \in E} \alpha_i \cdot \left(e^{t\mathbf{Q}} \right)_{i,j} \cdot q_j \Delta t + o(\Delta t) \right\}.
 \end{aligned} \tag{19}$$

Observing that $\sum_{w \in W} p_w(t) + \sum_{f \in F} p_f(t) = 1$ and

$$\sum_{i \in E} \sum_{j \in E} \alpha_i \left(e^{t\mathbf{Q}} \right)_{i,j} q_j \Delta t = \sum_{w \in W} p_w(t) q_w \Delta t + \sum_{f \in F} p_f(t) q_f \Delta t,$$

and after some algebraic manipulations, we get

$$\begin{aligned}
 \text{roi}(t) &= \lim_{\Delta t \rightarrow 0} \frac{1}{\Delta t} \left\{ \sum_{w \in W} p_w(t) \sum_{W \ni w_1 \neq w} q_{w,w_1} \Delta t + \sum_{f \in F} p_f(t) \sum_{F \ni f_1 \neq f} q_{f,f_1} \Delta t + o(\Delta t) \right\} \\
 &= \sum_{w \in W} p_w(t) \sum_{W \ni w_1 \neq w} q_{w,w_1} + \sum_{f \in F} p_f(t) \sum_{F \ni f_1 \neq f} q_{f,f_1} \\
 &= \sum_{i \in E} \sum_{w \in W} \sum_{W \ni w_1 \neq w} \alpha_i \left(e^{t\mathbf{Q}} \right)_{i,w} q_{w,w_1} + \sum_{i \in E} \sum_{f \in F} \sum_{F \ni f_1 \neq f} \alpha_i \left(e^{t\mathbf{Q}} \right)_{i,f} q_{f,f_1}.
 \end{aligned}$$

The proof is complete.

It may be useful to represent the previous indicators in vectorial notation. To this end, we define the vectors

$$\forall w \in W, \quad \bar{Q}_w := \sum_{f \in F} q_{w,f}, \quad \bar{\mathbf{Q}}_W = (\bar{Q}_w)_{w \in W}, \tag{20}$$

$$\forall f \in F, \quad Q_f := \sum_{w \in W} q_{f,w}, \quad \mathbf{Q}_F = (Q_f)_{f \in F}, \tag{21}$$

$$\forall w \in W, \quad {}_w Q_w := \sum_{w_1 \in W, w_1 \neq w} q_{w,w_1}, \quad {}_w \mathbf{Q} = ({}_w \bar{Q})_{w \in W}, \tag{22}$$

$$\forall f \in F, \quad {}_f\bar{\mathbf{Q}} := \sum_{f_1 \in F, f_1 \neq f} q_{f, f_1}, \quad \mathbf{F}\bar{\mathbf{Q}} = ({}_f\bar{\mathbf{Q}})_{f \in F}. \quad (23)$$

The ROCOF, ROCOR, and ROI indexes can be represented using the scalar product as follows:

$$rof(s) = \langle \mathbf{p}_W(s), \bar{\mathbf{Q}}_W \rangle, \quad ror(s) = \langle \mathbf{p}_F(s), \mathbf{Q}_F \rangle, \quad roi(s) = \langle \mathbf{p}_W(s), \mathbf{W}\mathbf{Q} \rangle + \langle \mathbf{p}_F(s), \mathbf{F}\bar{\mathbf{Q}} \rangle, \quad (24)$$

where $\mathbf{p}_W(s) = (p_w(s))_{w \in W}$ and $\mathbf{p}_F(s) = (p_f(s))_{f \in F}$ are the vectors of the unconditional probability at time s in the working and failure subsets of states, respectively.

Remark 1. The formulas in equation (24) include two special cases that should be referred to separately. The first case is where $s = 0$. At the initial time, $\mathbf{p}_W(0) = \alpha_W$ and $\mathbf{p}_F(0) = \alpha_F$, that is, the unconditional probability function coincides with the initial probability distribution. The indexes can be expressed according to

$$rof(s) = \langle \alpha_W(s), \bar{\mathbf{Q}}_W \rangle, \quad ror(s) = \langle \alpha_F(s), \mathbf{Q}_F \rangle, \quad roi(s) = \langle \alpha_W(s), \mathbf{W}\mathbf{Q} \rangle + \langle \alpha_F(s), \mathbf{F}\bar{\mathbf{Q}} \rangle.$$

The previous relationships allow for a quick comparison between the indexes. As an example, if

$$\langle \alpha_W(s), \bar{\mathbf{Q}}_W \rangle \geq \langle \alpha_F(s), \mathbf{Q}_F \rangle$$

we immediately realize that $rof(0) \geq ror(0)$ and from the continuity of these indexes with respect to time, we know that there exists a right neighborhood of $s = 0$, namely $I^+(0)$ such that $\forall t \in I^+(0), rof(t) \geq ror(t)$.

The second case is where $s \rightarrow \infty$. In the stationary case, the unconditional probability functions coincide with the stationary distribution of the Markov chain, that is, $\mathbf{p}_W(\infty) = \mathbf{L}_W$ and $\mathbf{p}_F(\infty) = \mathbf{L}_F$. The limiting probability vector $\mathbf{L} = [\mathbf{L}_W, \mathbf{L}_F]$ has a generic element

$$L_j = \frac{\pi_j / \sum_{h \neq j} q_{j, h}}{\sum_{i \in E} (\pi_i / \sum_{h \neq i} q_{i, h})},$$

where $\boldsymbol{\pi} = (\pi_1, \dots, \pi_s)$ is the limiting probability vector of the embedded Markov chain in the Markov process.

Thus, the indexes become

$$rof(\infty) = \langle \alpha_L, \bar{\mathbf{Q}}_W \rangle, \quad ror(\infty) = \langle \mathbf{L}_F, \mathbf{Q}_F \rangle, \quad roi(\infty) = \langle \mathbf{L}_W, \mathbf{W}\mathbf{Q} \rangle + \langle \mathbf{L}_F, \mathbf{F}\bar{\mathbf{Q}} \rangle.$$

The previous relationships allow for a quick comparison between the indexes in the asymptotic case. As an example, if

$$\langle \mathbf{L}_W, \bar{\mathbf{Q}}_W \rangle \geq \langle \mathbf{L}_F, \mathbf{Q}_F \rangle$$

we immediately realize that $rof(\infty) \geq ror(\infty)$ and from the continuity of these indexes with respect to time, we know that there exists a neighborhood of infinity, namely $I(\infty) = (M, \infty)$ such that $\forall t \in I(\infty), rof(t) \geq ror(t)$.

The next result establishes a relationship among the three indexes.

Proposition 7. *The ROCOF, the ROCOR, and the ROI functions of a Markov process of generator matrix \mathbf{Q} and vector of initial probabilities $\boldsymbol{\alpha}$ satisfy the next relation:*

$$roi(t) + rof(t) + ror(t) = \sum_{i \in E} \sum_{h \in E} \alpha_i (e^{t\mathbf{Q}})_{i, h} \sum_{j \neq h} q_{h, j}. \quad (25)$$

PROOF. Equation (10) can be arranged so that:

$$roi(t) = \sum_{i \in E} \left(\sum_{w \in W} \sum_{w_1 \in W} \alpha_i (e^{t\mathbf{Q}})_{i, w} \cdot q_{w, w_1} + \sum_{f \in F} \sum_{f_1 \in F} \alpha_i (e^{t\mathbf{Q}})_{i, f} \cdot q_{f, f_1} \right)$$

$$\begin{aligned}
 &= \left[\sum_{i \in E} \sum_{w \in W} \alpha_i(e^{Qt})_{i,w} \right] (-q_{w,w} - \sum_{f \in F} q_{w,f}) + \left[\sum_{i \in E} \sum_{f \in F} \alpha_i(e^{Qt})_{i,f} \right] (-q_{f,f} - \sum_{w \in W} q_{f,w}) \\
 &= \left[\sum_{i \in E} \sum_{w \in W} \alpha_i(e^{Qt})_{i,w} \right] (-q_{w,w}) - \text{rof}(t) + \left[\sum_{i \in E} \sum_{f \in F} \alpha_i(e^{Qt})_{i,f} \right] (-q_{f,f}) - \text{ror}(t),
 \end{aligned}$$

where the last equality is obtained using equations (6) and (8).

Relation (25) follows by elementary algebraic calculations after having observed that $q_{w,w} = -\sum_{j \neq w} q_{w,j}$ and $q_{f,f} = -\sum_{j \neq f} q_{f,j}$.

The previous proposition suggests the definition of a fourth index that coincides with the right-hand side of equation (25). Indeed, we can define a total mobility rate at time t according to the next formula:

$$\text{tmr}(t) := \sum_{i \in E} \sum_{h \in E} \alpha_i(e^{tQ})_{i,h} \sum_{j \neq h} q_{h,j}.$$

The total mobility rate at a time t provides the entire attitude of the system to experience any type of transition in the infinitesimal interval $(t, t + \Delta t)$.

Remark 2. It is worth noticing that the total mobility rate is not dependent on the partition of the phase space in the working and failure states. Thus, the function $\text{tmr}(t)$ expresses a description of the mobility of the considered Markov process independently of the classification of its states in work and failure. Clearly, its components ($\text{rof}(t)$, $\text{ror}(t)$, $\text{roi}(t)$) study the different aspects of the entire mobility according to the typology of transitions depending on the partition of the state space.

Remark 3. The total mobility rate index includes a well-known mobility index for continuous-time Markov chains. Indeed, its asymptotic behavior coincides with the so-called expected rate of moving from one state to another (see Geweke, Marshall, and Zarkin (1986) for an in-depth discussion):

$$\lim_{t \rightarrow \infty} \text{tmr}(t) = \lim_{t \rightarrow \infty} \sum_{i \in E} \sum_{h \in E} \alpha_i(e^{tQ})_{i,h} \sum_{j \neq h} q_{h,j} = \sum_{h \in E} L_h \sum_{j \neq h} q_{h,j} = - \sum_{h \in E} L_h q_{h,h}.$$

Therefore, we end up with a function that describes the entire time evolution of the mobility process and not only the single value represented by its asymptotic score.

3. Mobility indices applied to wind farm

Wind energy production is inherently affected by the stochastic variability of wind speed, both over short and long timescales. This variability influences not only the amount of energy generated, but also the operational reliability and the maintenance requirements of wind turbines. In particular, frequent transitions between wind regimes, as well as prolonged periods of calm or turbulence, can significantly impact the stress profiles of components and the overall system wear.

Traditional reliability measures based on long-term averages or aggregated failure counts (e.g., Weibull parameters or ROCOF) may fail to capture the nuanced dynamics induced by such variability. For this reason, we propose the application of time-dependent mobility indicators—including ROCOF, ROCOR, ROI, and TMR—as a complementary set of tools to characterize the instantaneous behavior of wind farms.

In this chapter, we illustrate how these indicators can be computed from real wind speed data using a continuous-time Markov model, and we demonstrate their empirical relevance through a comparative analysis of 18 large-scale wind farms located in different climatic zones. The goal is to identify and classify different reliability logics—ranging from persistence-dominated to transition-intensive dynamics—thereby providing insights useful for both design and operational decision-making in the wind energy sector.

3.1. Database description

The empirical analysis is based on **hourly wind-speed time series at 50 m above ground level (WS_{50M}) for 18 large wind farms world-wide** (Fig. 1). For each plant the nearest grid point of the *Modern-Era Retrospective analysis for Research and Applications, version 2* (MERRA-2) re-analysis produced by NASA's Global Modeling and Assimilation Office. No missing values were encountered; the few negative or $> 50 \text{ m s}^{-1}$ outliers ($< 0.01 \%$) were discarded.

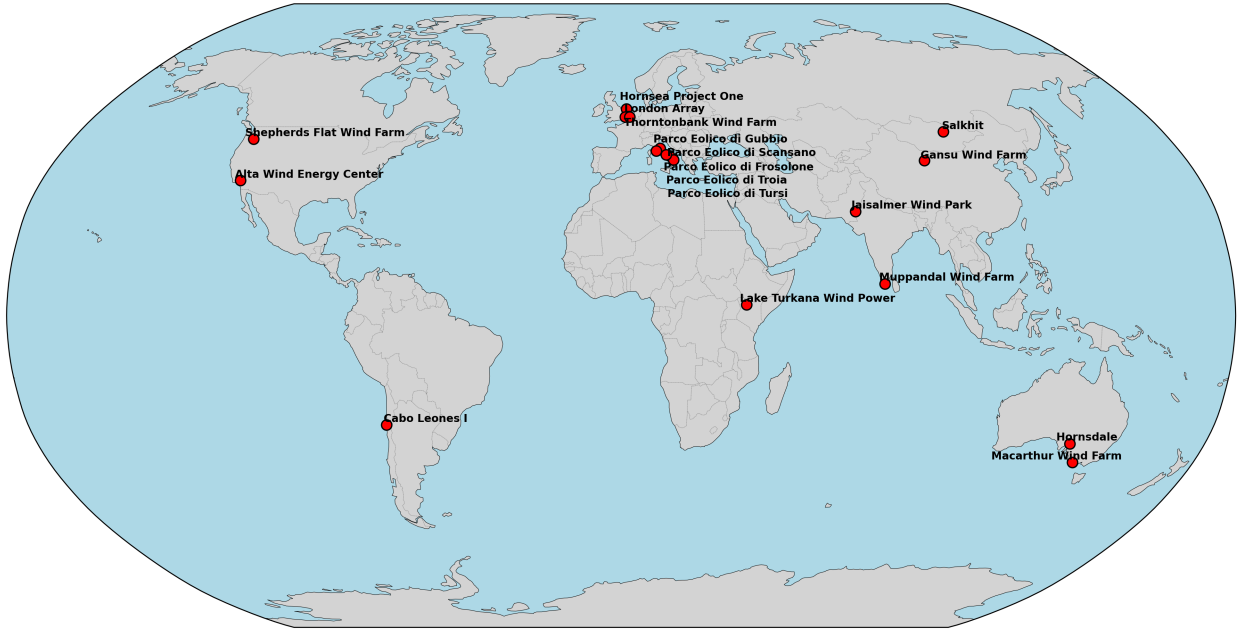


Figure 1: Geographical distribution of the 18 wind farms analysed.

- **Spatial coverage** – 18 on-shore and off-shore facilities located in 10 countries on five continents (United States, Chile, China, Australia, United Kingdom, India, Kenya, Italy, Mongolia, Belgium).
- **Temporal coverage** – 1 January 2016 – 21 April 2025 (81 576 hourly records per site, $N = 1\,468\,368$ observations in total).
- **Variable** – WS_{50M} (m/s); original MERRA-2 resolution is $0.5^\circ \times 0.625^\circ$ ($\approx 50\text{--}60$ km).

For reliability modelling, each series was discretised into 11 equally-spaced states $E = \{0, \dots, 10\}$ of width 2 m s^{-1} , spanning $0\text{--}20 \text{ m s}^{-1}$ (the last state includes all wind speed values greater than 20 m s^{-1}). The hourly histograms were fitted with a two-parameter Weibull density via maximum likelihood; Fig. 2 shows the empirical distributions and the fitted curves.

The fitted parameters highlight a pronounced heterogeneity among the selected sites (see table 1). Scale factors λ span almost a twofold range ($4.97\text{--}9.90 \text{ m s}^{-1}$), reflecting climates that vary from low-wind inland locations (e.g. Frosolone) to energetic off-shore settings (Hornsea). Shape coefficients k show an even wider dispersion: Lake Turkana ($k = 4.13$) exhibits a very narrow, quasi-Gaussian speed distribution, whereas Frosolone's $k = 1.62$ denotes a highly skewed regime dominated by light winds. Such diversity confirms that reliability indicators derived from these data cannot rely on a single generic wind model but must account for site-specific wind-speed dynamics.

3.2. Markov modelling of the wind-speed series

Let $\{J_n\}_{n \geq 0}$ be the discrete-time chain obtained by classifying each hourly wind-speed observation into the 11 equi-spaced states introduced in Sect. 3.1. For every pair of states (i, j) we count the number of successive occurrences

$$N_{ij} = \left| \{n : J_n = i, J_{n+1} = j\} \right|,$$

ignoring the final (possibly incomplete) segment of each day so as to keep the sampling interval fixed at $\Delta t = 1 \text{ h}$. The empirical *embedded* transition probabilities are then

$$p_{ij} = \frac{N_{ij}}{\sum_k N_{ik}}, \quad i, j \in \{0, \dots, 10\}.$$

ROCOF

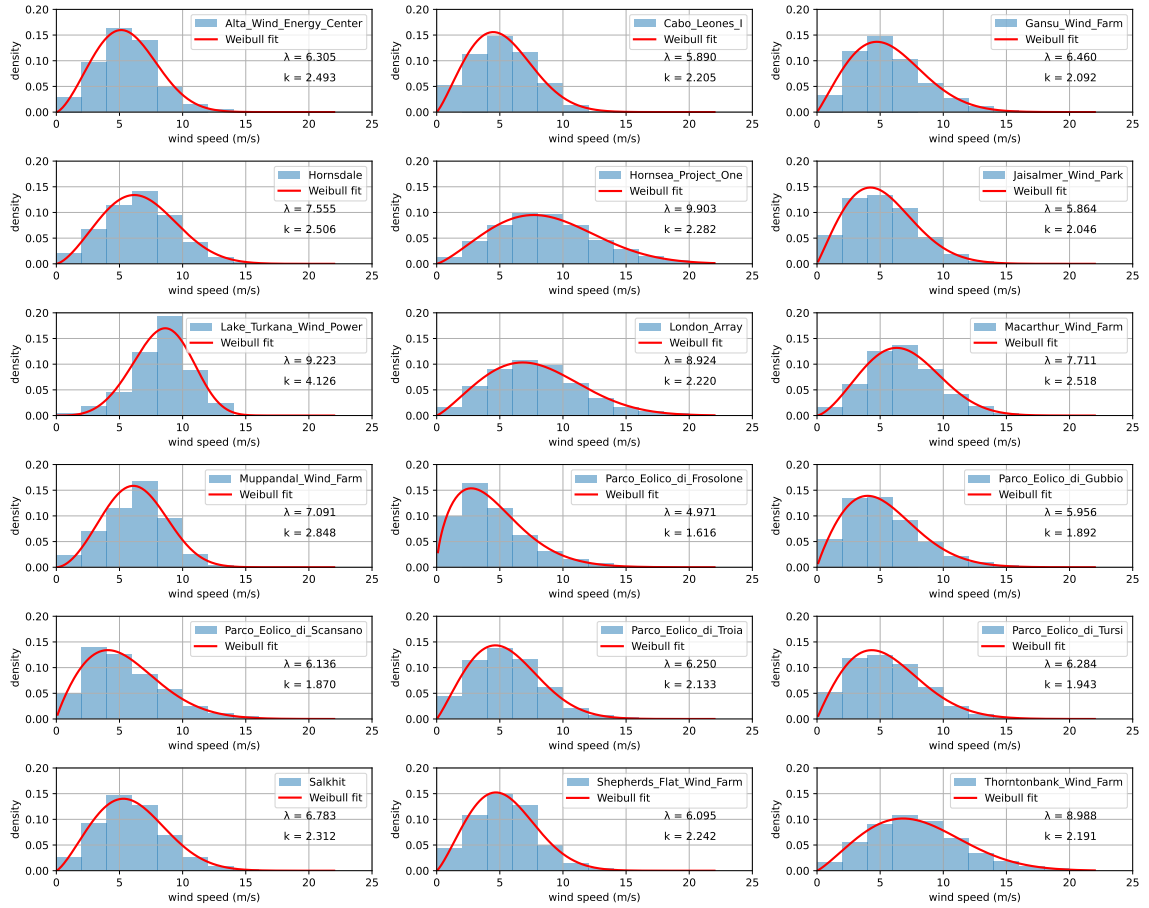


Figure 2: Hourly wind-speed histograms (bars) and fitted Weibull densities (lines) for each site.

The resulting matrix is displayed in Fig. 3, it is strongly diagonal-dominant, as expected for an hourly sampling, and shows that most transitions occur between neighbouring wind regimes, while jumps of more than two classes are virtually absent.

In our empirical analysis, wind states are derived from time series of wind speed data recorded at hourly intervals. For each hour, we compute the average wind speed and classify it into one of the predefined discrete states, effectively obtaining a periodically sampled discrete-time trajectory. This leads naturally to the estimation of a first-order time-homogeneous discrete-time Markov chain.

In order to analyze the dynamics in continuous time—and to compute time-continuous mobility indicators such as ROCOF and ROI—we embed the observed transition matrix into a continuous-time Markov process. This is achieved by solving a matrix logarithm problem: given the hourly transition probability matrix \mathbf{P} , we compute a generator matrix \mathbf{Q} (shown in Fig. 4) such that $\mathbf{P} \approx e^{\mathbf{Q}\Delta t}$ with $\Delta t = 1$ hour. The generator matrix \mathbf{Q} is then used to obtain the transient distribution and evaluate time-dependent indicators across different time scales.

3.3. Time evolution of the four mobility indicators

In order to apply the mobility indicators to a reliability framework, the state space must be partitioned into working and failure states. This classification is guided by the typical power curve of commercial wind turbines, which produce energy only within a specific wind speed range—typically between the cut-in and cut-out thresholds.

In our analysis, states are defined on a discrete scale from 0 to 10, each representing a wind speed class. Based on standard operational limits, we classify as *working states* the intermediate wind classes 2 through 8, which correspond to wind speeds that generally fall within the operational range of most utility-scale turbines. Conversely, states 0 and

Table 1
Weibull scale (λ) and shape (k) parameters estimated for each of the 18 wind farms.

Site	λ (m s ⁻¹)	k
Alta_Wind_Energy_Center	6.31	2.49
Cabo_Leones_I	5.89	2.21
Gansu_Wind_Farm	6.46	2.09
Hornsedale	7.55	2.51
Hornsea_Project_One	9.90	2.28
Jaisalmer_Wind_Park	5.86	2.05
Lake_Turkana_Wind_Power	9.22	4.13
London_Array	8.92	2.22
Macarthur_Wind_Farm	7.71	2.52
Muppandal_Wind_Farm	7.09	2.85
Parco_Eolico_di_Frosolone	4.97	1.62
Parco_Eolico_di_Gubbio	5.96	1.89
Parco_Eolico_di_Scansano	6.14	1.87
Parco_Eolico_di_Troia	6.25	2.13
Parco_Eolico_di_Tursi	6.28	1.94
Salkhit	6.78	2.31
Shepherds_Flat_Wind_Farm	6.09	2.24
Thorntonbank_Wind_Farm	8.99	2.19

1 (very low wind) and 9–10 (very high wind) are categorized as *failure states*, since turbines are either unable to start or are forced to shut down to prevent mechanical stress or damage.

In the set of figures 5-8 we show the time evolution of the four indicators, defined above, estimated for the 18 sites under analysis. More specifically, we emphasize the transient behavior of the indices, their dependence from the initial state and the differences between sites.

Figure 5 follows the first two days after the process is forced to start in the calmest wind class (0–2 m s⁻¹), i.e. from an initial *failure* state for power production. Although every curve originates from the same unfavourable state, they separate almost immediately, and the way they diverge encapsulates the wind–climate fingerprint of each site.

Figure 5 offers a dynamic portrait of how wind farms evolve over time following an initial calm condition. In the first few hours, the mobility is driven primarily by lateral movements within the failure region (reflected in high ROI) and upward transitions into productive states (captured by ROCOR). These early movements yield moderate-to-high values of total mobility rate $TMR(t)$, particularly in sites with variable winds near the cut-in threshold, such as Frosolone and Gubbio.

As time progresses, the system tends to settle temporarily into working states. This leads to a shift in dynamics: repair events become less frequent, while the risk of falling back into failure conditions increases. Consequently, $ROCOR(t)$ decreases, $ROCOF(t)$ rises, and $ROI(t)$ reflects internal fluctuations within each subset. The combined effect results in a broad $TMR(t)$ peak—early and lower for stable, energetic climates like Hornsea and Lake Turkana; later and higher for sites with intermittent, weak winds.

After the first day, all rates gradually converge to their long-run values. Some farms settle on low TMR_{∞} levels, indicative of persistent operation within the working subset, while others maintain a high long-term mobility, reflecting frequent transitions across operational thresholds. Importantly, these asymptotic behaviors are not fully captured by the Weibull parameters alone: farms with similar (λ, k) pairs can exhibit markedly different mobility profiles. This highlights the added value of TMR and related indicators in distinguishing the intrinsic dynamical features of wind regimes.

In essence, the TMR curve encapsulates the operational rhythm of each site. Early peaks suggest brief turbulence followed by stability, whereas sustained high levels signal chronic transitions in and out of production. The indicators thus provide actionable insights for maintenance planning and grid integration.

3.4. Time evolution of the four mobility indicators: alternative initial conditions

When the process starts in a lower working state—such as state 2, corresponding to moderate wind conditions around 4–6 m/s—the turbine is technically within its operational range, but near the threshold of failure. As shown in Figure 6, the early evolution is dominated by a high rate of failure (ROCOF), reflecting the strong likelihood of wind speeds dropping below cut-in and thus exiting the productive set. The rate of recovery (ROR) begins near zero and reaches a brief peak within the first hour, associated with possible returns from the adjacent failure states. Total mobility (TMR) declines as the system stabilizes and diffuses across neighboring classes. However, the nature and pace of this transition vary significantly between sites.

A different behavior is observed when the system starts near the center of the operational range—specifically state 6, corresponding to wind speeds around 12–14 m/s—as in Figure 7. In this scenario, the turbines operate near their aerodynamic optimum, and the system exhibits a mild and balanced response. ROCOF and ROR increase moderately in the early hours but remain closely matched, suggesting that failures and repairs occur with similar likelihood. In this case, the rate of inoccurrence (ROI) dominates the dynamics, highlighting the process’s tendency to remain within the productive subset. Total mobility starts high but decays slowly, sustained by internal transitions among working states.

The most asymmetric situation arises when the initial condition is a failure state above the cut-out threshold—specifically state 10, with wind speeds exceeding 20 m/s—as shown in Figure 8. Here, by construction, ROCOF is initially zero, and the early mobility is entirely driven by the rate of recovery (ROR), which spikes sharply as the system attempts to re-enter the working set. In sites like Gansu, characterized by frequent gusts and sharp reversals, ROR quickly reaches a peak above 0.11 h^{-1} , but is soon followed by sustained ROCOF, indicating that repairs are often short-lived and failures recur rapidly. Conversely, in lower-wind sites like Frosolone, the system is more likely to stabilize once it returns to the operational zone: repairs are more effective, and subsequent failures are less frequent, leading to a smoother decline in mobility.

3.5. Synthesis and added value with respect to the Weibull fit

The comparative analysis illustrated in Figures 6 to 8 highlights a key contribution of this framework: the proposed mobility indicators provide a time-resolved and direction-sensitive view of wind variability that cannot be inferred from the static characterization offered by a Weibull fit. While the parameters λ and k remain useful for describing the general shape and scale of the wind speed distribution, they offer no indication of how the system evolves dynamically—how frequently it crosses operational thresholds, how persistently it remains in productive states, or how sharply it reacts to extreme conditions.

In contrast, the Markov-based indicators dissect the process into its essential components. The inoccurrence rate (ROI) reflects the system’s ability to remain operational once inside the productive set, capturing retention properties that may differ substantially between sites with otherwise similar Weibull parameters. The rates of failure (ROCOF) and recovery (ROR) quantify the asymmetry of transitions across the working/failure boundary, making it possible to distinguish between systems prone to frequent shutdowns and those capable of rapid recovery. The total mobility rate (TMR), as the sum of these three contributions, serves as an aggregate measure of state-space churn, highlighting the overall dynamism of each site in response to stochastic wind fluctuations.

These indicators do not merely describe qualitative tendencies—they provide actionable information on the timing and intensity of transitions. For example, Figure 6 shows that when the system starts from a marginal working state, failure is initially dominant and recovery is delayed; in Figure 7, we observe a stable internal dynamic near the operational center, with ROI sustaining a long-lasting mobility shoulder; while Figure 8 reveals the instability of conditions above cut-out, where high ROR is often counteracted by a rapid resurgence of ROCOF. These dynamic patterns would remain invisible in a Weibull-only analysis, which treats time implicitly and offers no directional breakdown of state transitions.

In summary, the mobility indicators extend the description of wind regimes from static potential to dynamic behavior. They enable the quantification not only of how often a wind farm will experience problematic conditions, but also of how quickly it will enter, recover from, or oscillate between them. This level of granularity supports the development of operational strategies that are not just site-specific, but also time-adaptive—helping operators anticipate, respond to, and mitigate the effects of wind variability with greater precision.

3.6. Mobility surfaces for two contrasted parks

Figures 9 and 10 illustrate the full temporal evolution—over a 72-hour horizon—of the four mobility indicators (ROI, ROCOF, ROCOR, and TMR) for two representative wind farms: Gansu (China) and Muppandal (India).

These sites were selected due to their contrasting operational behaviors, despite displaying relatively similar Weibull parameters: both have shape factors near $k \approx 2.5$, and their scale parameters differ by less than 15%. Yet, their long-run total mobility rates diverge significantly—about 0.30 h^{-1} for Gansu versus only 0.11 h^{-1} for Muppandal—revealing fundamentally different reliability profiles.

The Gansu Wind Farm, located on a continental high plateau, displays a mobility regime dominated by persistence. As shown in Figure 9, the ROI surface rapidly forms a broad, stable plateau, with values between 0.22 and 0.28 h^{-1} regardless of the initial state. This indicates that the system, once inside the working or failure subset, tends to remain there for extended periods. The directional indicators ROCOF and ROCOR emerge briefly and locally, particularly when starting from the extreme classes, but they decay quickly within the first few hours. As a result, the TMR surface settles into a flat and elevated region, suggesting that mobility in Gansu is largely shaped by long holding times rather than frequent transitions across the operational boundary.

In contrast, Muppandal, shaped by a monsoon gap-flow regime, exhibits a mobility profile driven by rapid directional transitions. As seen in Figure 10, ROI starts high only in the lowest wind class but quickly declines across all states, eventually stabilizing at much lower values (0.06 – 0.08 h^{-1}). When starting from near cut-out speeds, ROI remains essentially zero throughout. ROCOF and ROCOR are both weaker than in Gansu, and their transient peaks are narrow and short-lived, disappearing after just a few hours. TMR in Muppandal follows a similar pattern: a short-lived ridge forms in the early hours but rapidly collapses into a flat surface below 0.12 h^{-1} . The picture that emerges is one of volatility concentrated in short bursts, where failures and recoveries alternate quickly and without persistence.

These two contrasting cases underscore the operational implications of mobility analysis. Gansu's persistence implies that maintenance planning can be scheduled over longer time windows, as the system tends to remain stable within its current regime. Muppandal, instead, demands more responsive strategies: the short duration of each event requires readiness on minute-to-hour scales, especially to handle erratic transitions and sudden availability drops. From a grid support perspective, Gansu offers large but predictable flexibility margins, while Muppandal calls for fast-reacting, low-capacity reserves.

4. Conclusions

This work has introduced a new family of time-dependent indicators—ROCOR, ROI, and TMR—to complement the classical Rate of Occurrence of Failures (ROCOF) in the analysis of Markov systems. These mobility-based metrics offer a dynamic and directional view of system behavior, capturing not only how often failures or repairs occur, but also how persistently the system remains within operational or failed states, and how intensely it shifts between them.

Applied to a global dataset of wind farms, the proposed framework revealed patterns that traditional static measures, such as the Weibull distribution, are unable to detect. While two sites may appear similar under a static fit, their mobility profiles often expose profound differences in operational rhythm, recovery potential, and failure volatility. The ability to quantify not just the likelihood but also the pace and direction of state transitions allows for a far more nuanced and operationally relevant assessment of reliability.

By turning state-based modeling into a temporal narrative, these indicators open new possibilities for anticipating critical time windows, optimizing maintenance and resource allocation, and tailoring responses to site-specific dynamics. The empirical results demonstrate that TMR and its components capture the intrinsic logic of system evolution—whether driven by persistence or transition—in a way that enhances both theoretical understanding and practical decision-making.

In essence, this mobility-based perspective complements traditional characterizations of complex systems by focusing not only on their state distribution, but also on the dynamics of their transitions. The evidence presented suggests that such indicators hold broad potential across reliability theory and related fields where time-sensitive behavior matters.

References

- W. R. Blischke, D. P. Murthy, *Reliability: modeling, prediction, and optimization*, John Wiley & Sons, 2011.
- V. S. Barbu, N. Limnios, *Semi-Markov chains and hidden semi-Markov models toward applications: their use in reliability and DNA analysis*, volume 191, Springer Science & Business Media, 2009.
- I. A. Ushakov, *Probabilistic reliability models*, John Wiley & Sons, 2012.
- M. V. Koutras, On a markov chain approach for the study of reliability structures, *Journal of Applied Probability* 33 (1996) 357–367.
- N. Limnios, G. Oprisan, *Semi-Markov processes and reliability*, Springer Science & Business Media, 2001.
- A. Csenki, On the interval reliability of systems modelled by finite semi-markov processes, *Microelectronics Reliability* 34 (1994) 1319–1335.

- A. Csenki, An integral equation approach to the interval reliability of systems modelled by finite semi-markov processes, *Reliability engineering & system safety* 47 (1995) 37–45.
- S. Georgiadis, N. Limnios, Interval reliability for semi-markov systems in discrete time, *Journal de la Société Française de Statistique* 155 (2014) 152–166.
- S. Georgiadis, N. Limnios, Nonparametric estimation of interval reliability for discrete-time semi-markov systems, *Journal of Statistical Theory and Practice* 10 (2016) 20–39.
- V. S. Barbu, G. D'Amico, T. Gkelsinis, Sequential interval reliability for discrete-time homogeneous semi-markov repairable systems, *Mathematics* 9 (2021) 1997.
- G. D'Amico, T. Gkelsinis, On a mixed transient–asymptotic result for the sequential interval reliability for semi-markov chains, *Mathematics* 12 (2024) 1842.
- A. Platis, N. Limnios, M. Le Du, Dependability analysis of systems modeled by non-homogeneous markov chains, *Reliability Engineering & System Safety* 61 (1998) 235–249.
- N. Limnios, Dependability analysis of semi-markov systems, *Reliability Engineering & System Safety* 55 (1997) 203–207.
- G. D'Amico, J. Janssen, R. Manca, Initial and final backward and forward discrete time non-homogeneous semi-markov credit risk models, *Methodology and Computing in Applied Probability* 12 (2010) 215–225.
- G. D'Amico, R. Manca, F. Petroni, D. Selvamuthu, On the computation of some interval reliability indicators for semi-markov systems, *Mathematics* 9 (2021) 575.
- K. Yang, J. Xue, Continuous state reliability analysis, in: *Proceedings of 1996 Annual Reliability and Maintainability Symposium, IEEE, 1996*, pp. 251–257.
- G. D'Amico, Age-usage semi-markov models, *Applied Mathematical Modelling* 35 (2011) 4354–4366.
- N. Limnios, Reliability measures of semi-markov systems with general state space, *Methodology and Computing in Applied Probability* 14 (2012) 895–917.
- L. Yeh, Calculating the rate of occurrence of failures for continuous-time markov chains with application to a two-component parallel system, *Journal of the Operational Research Society* 46 (1995) 528–536.
- B. Ouhbi, N. Limnios, The rate of occurrence of failures for semi-markov processes and estimation, *Statistics & probability letters* 59 (2002) 245–255.
- G. D'Amico, Rate of occurrence of failures (rocof) of higher-order for markov processes: analysis, inference and application to financial credit ratings, *Methodology and Computing in Applied Probability* 17 (2015) 929–949.
- G. D'Amico, F. Petroni, Rocof of higher order for semi-markov processes, *Applied Mathematics and Computation* 441 (2023) 127719.
- G. D'Amico, F. Gismondi, Recent developments in the computation of the rocof of multi-state systems and its applications, *Reliability theory & applications* 1 (77) (Vol.19) (2024).
- M. Bruneau, S. E. Chang, R. T. Eguchi, G. C. Lee, T. D. O'Rourke, A. M. Reinhorn, M. Shinozuka, K. Tierney, W. A. Wallace, D. Von Winterfeldt, A framework to quantitatively assess and enhance the seismic resilience of communities, *Earthquake Spectra* 19 (2003) 733–752.
- N. Sharma, A. Tabandeh, P. Gardoni, Resilience analysis: A mathematical formulation to model resilience of engineering systems, *Sustainable and Resilient Infrastructure* 3 (2018) 49–67.
- R. Billinton, K. E. Bollinger, Transmission system reliability evaluation using markov processes, *IEEE Transactions on power apparatus and systems* (1968) 538–547.
- D. Banjevic, A. Jardine, Calculation of reliability function and remaining useful life for a markov failure time process, *IMA journal of management mathematics* 17 (2006) 115–130.
- A. Csenki, Joint interval reliability for markov systems with an application in transmission line reliability, *Reliability Engineering & System Safety* 92 (2007) 685–696.
- P. Brémaud, Gibbs fields and monte carlo simulation, *Markov Chains: Gibbs Fields, Monte Carlo Simulation, and Queues* (1999) 253–322.
- A. Sadek, N. Limnios, Nonparametric estimation of reliability and survival function for continuous-time finite markov processes, *Journal of Statistical Planning and Inference* 133 (2005) 1–21.
- S. Ding-hua, A new method for calculating the mean failure numbers of a repairable system during $(0, t)$, *Acta Mathematicae Applicatae Sinica* 8 (1985) 101–110.
- L. Yeh, The rate of occurrence of failures, *Journal of Applied Probability* 34 (1997) 234–247.
- J. Geweke, R. C. Marshall, G. A. Zarkin, Mobility indices in continuous time markov chains, *Econometrica: Journal of the Econometric Society* (1986) 1407–1423.

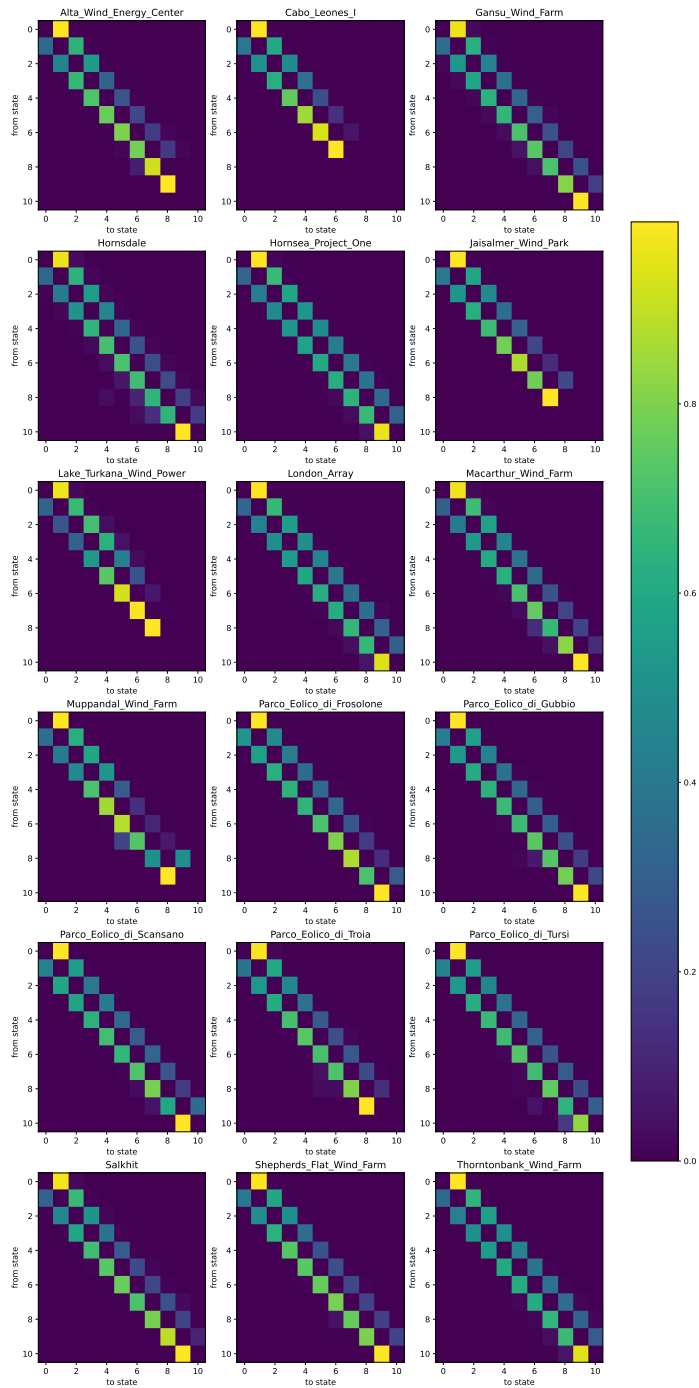


Figure 3: Hourly one-step transition-probability matrix $P = (p_{ij})$ obtained by classifying each observation into the 11 wind-speed states (2 m s^{-1} bins, $0 \geq 20 \text{ m s}^{-1}$). The strong main diagonal and its two nearest neighbours show that hour-to-hour changes seldom exceed $\pm 2 \text{ m s}^{-1}$, while the nearly symmetric pattern indicates the absence of any persistent upward or downward drift over the 2016–2025 window.

ROCOF

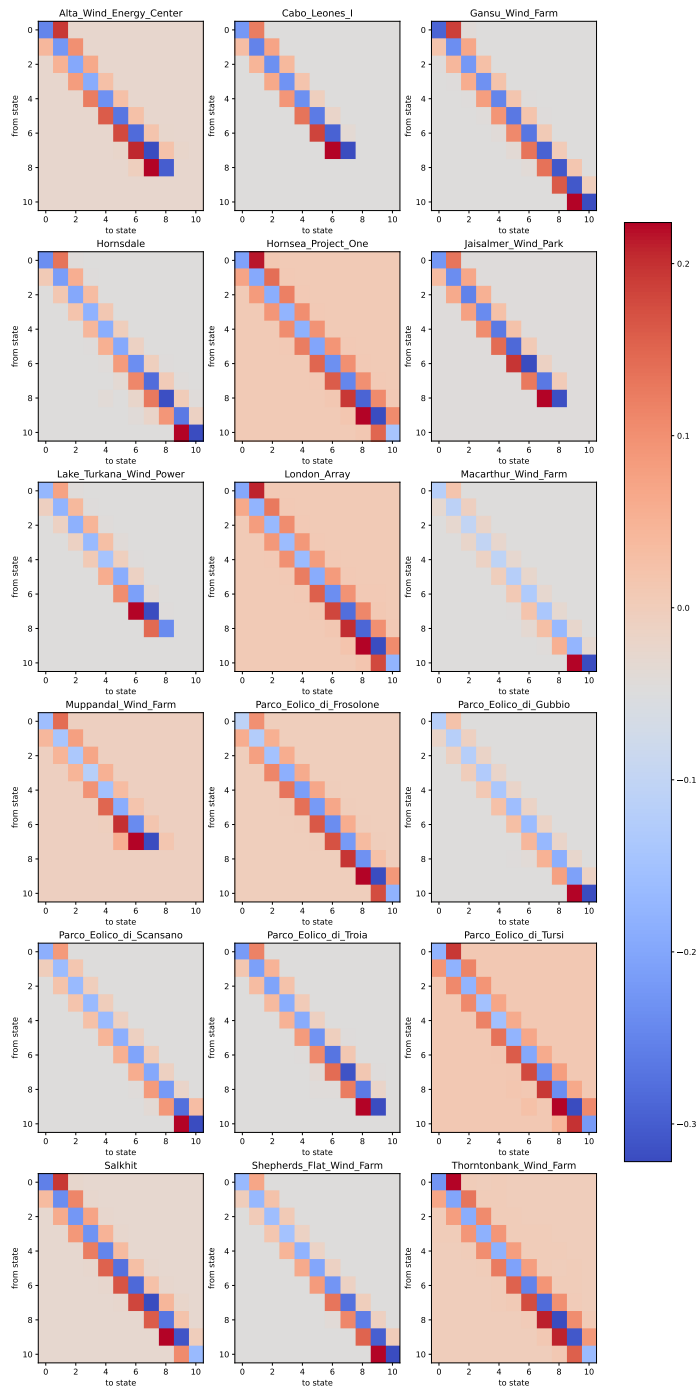


Figure 4: Continuous-time generator matrix $\mathbf{Q} = (q_{ij})$ (units: h^{-1}) derived from the embedded chain in Fig. 3. Off-diagonal intensities mirror the structure of \mathbf{P} but are rescaled by the shorter holding times of rare, high-speed states, making their contribution more prominent.

ROCOF

Initial state = 0

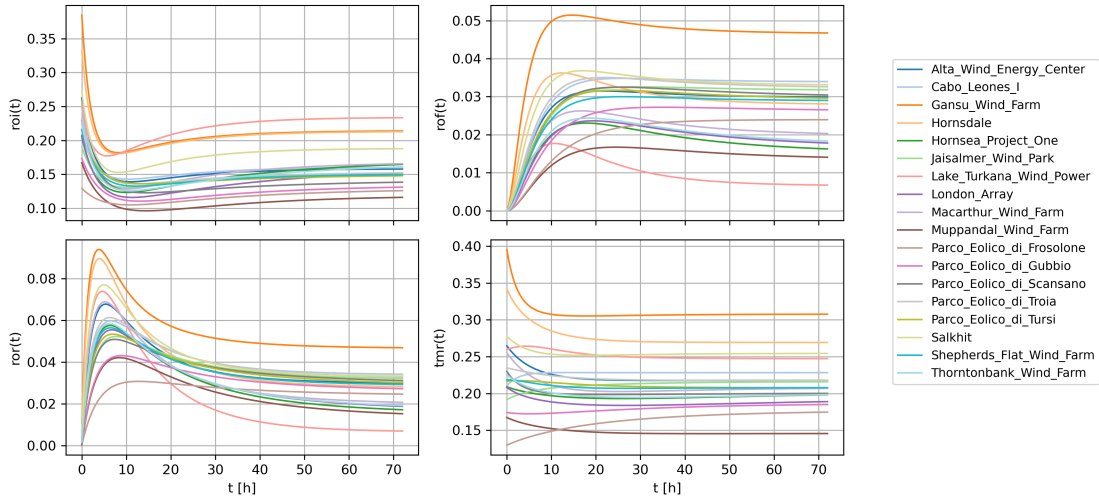


Figure 5: Temporal evolution of the four mobility indicators starting from a calm (failure) state (state 1). Sites differ markedly in their early repair dominance, timing of crossover, and long-run volatility, revealing distinct reliability dynamics not visible from static analysis.

Initial state = 2

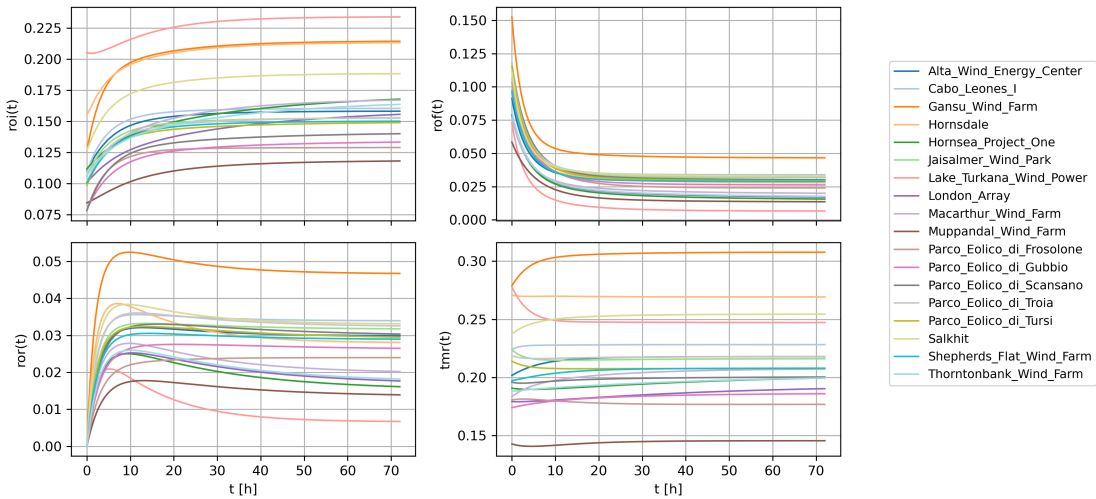


Figure 6: Mobility indicators starting from a lower working state (state 2, 4–6 m/s). The early dynamics are dominated by failures, with delayed and site-dependent recoveries. Long-run mobility reflects the system's ability to stabilize within productive classes.

ROCOF

Initial state = 6

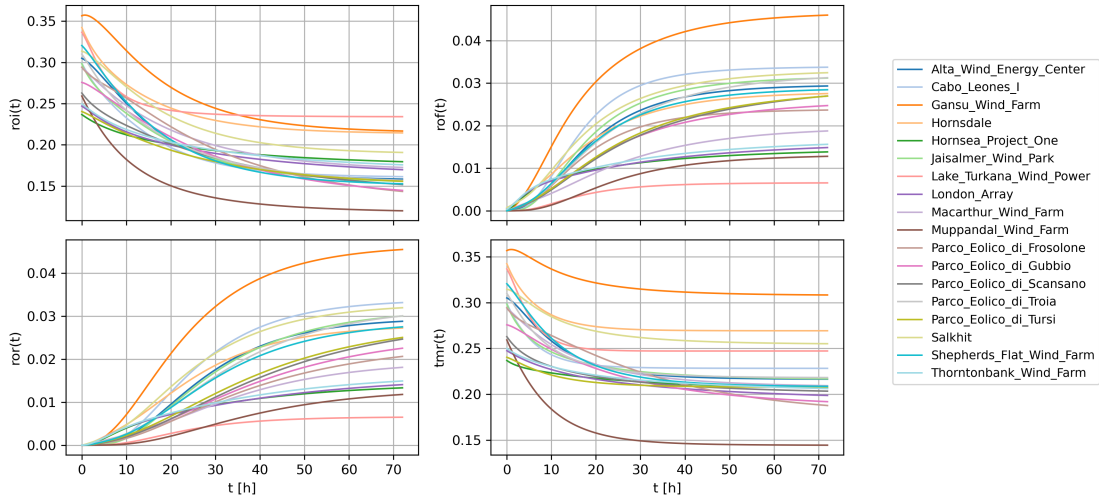


Figure 7: Mobility indicators starting near the center of the working range (state 6, 12–14 m/s). The system exhibits balanced, low-volatility dynamics with persistent ROI and mild transitions, highlighting intra-class motion rather than threshold crossings.

Initial state = 10

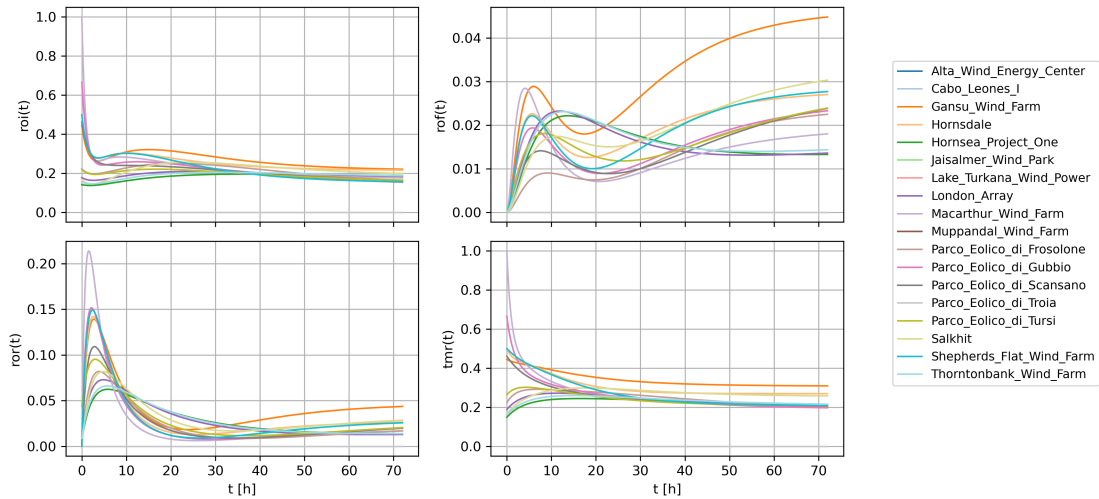


Figure 8: Mobility indicators starting in an upper failure state (state 10, >20 m/s). The early evolution is dominated by attempts to re-enter the working subset, with ROR spikes followed by renewed failures. Long-run mobility remains low and asymmetric across sites.

ROCOF

Site: Gansu_Wind_Farm

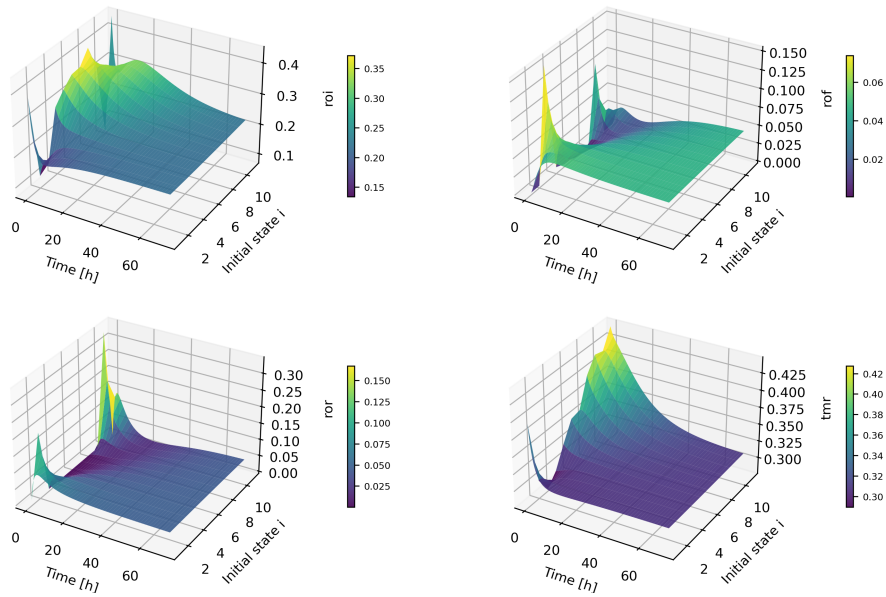


Figure 9: 72-hour mobility indicators at Gansu Wind Farm (persistence-driven regime)

Site: Muppandal_Wind_Farm

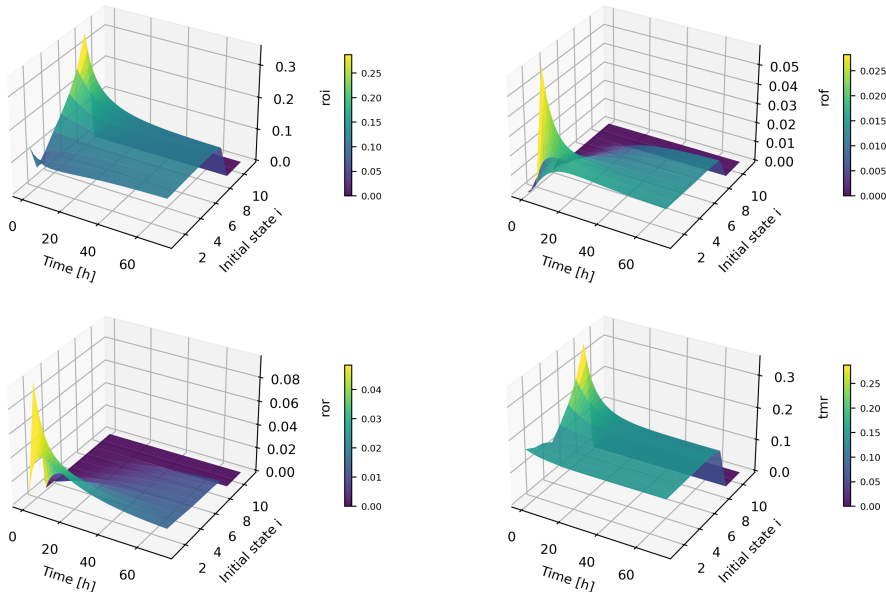


Figure 10: 72-hour mobility indicators at Muppandal Wind Farm (transition-driven regime)